034629-1-F

A Novel Millimeter-Wave, Low-Loss, Electronically Controlled Phase Shifter for Monolithic, Beam Steering Phased-Array Antenna Application

Kamal Sarabandi

March 1997

34629-1-F = RL-2470

A NOVEL MILLIMETER-WAVE, LOW-LOSS, ELECTRONICALLY CONTROLLED PHASE SHIFTER FOR MONOLITHIC, BEAM-STEERING PHASED-ARRAY ANTENNA APPLICATION

Final Report

ONR Code 313
Office of Naval Research
800 North Quincy Street
Arlington, VA 22217
Att: **Dr. W. Stachnik**

K. Sarabandi
Radiation Laboratory
Department of Electrical Engineering and Computer Science
The University of Michigan
Ann Arbor, MI 48109-2122
Tel: (313) 936-1575
Fax: (313) 747-2106

March 1997

1 Introduction

The purpose of this document is to summarize the accomplishments made on the project regarding construction of a millimeter-wave electronically controlled phase shifter funded by ONR under contract N00014-96-1-1120. Our activities in this pilot project can be categorized into two major areas: 1) theoretical analysis, and 2)experimental and development of fabrication methodology. Significant progress has been made in both areas during the very short period of the contract and details of our effort and related results are provided in the following sections.

2 Objective

This section provides a short description of the problem at hand and a list of itemized tasks needed for accomplishing the objective of the project. In this effort a new approach for the design of electronically controlled phase shifters appropriate for millimeter and submillimeter wavelengths was investigated. The fundamental concept for achieving phase shift is based on geometric deformation of the cross section of a waveguide structure supporting a traveling wave. Geometric deformation of a waveguide cross section modifies the cutoff frequency of the propagating mode which in turn changes the propagation constant. Therefore, imposing a certain deformation along a finite length of the waveguide will result in the desired phase shift. Micro-machining technology is proposed to construct the waveguide with a flexible membrane wall which can be displaced electronically. The plan was to use silicon wafers (in a specific crystalline orientation) and an anisotropic etchant such as EDP or TMAH to form a trapezoidal groove with the desired dimensions [?]. The groove was to be metallized and its open area will be covered with a thin dielectric membrane. Instead of using silicon wafer to construct the waveguide we used instead a metallic trapezoidal waveguide in this pilot study. The lower surface of the membrane facing the groove must first be metallized in order to form a trapezoidal waveguide as shown in Fig. 1. Electronically controlled displacement of the membrane is accomplished by employing

electrostatic forces.

In order to move the membrane electrostatically, a very small gap is required which was manufactured using silicon etching technology. Basically, another silicon wafer (conducting) is etched in a similar manner to form a groove with a slightly wider width and much shallower depth than the waveguide groove. This wafer will be placed on top of the other wafer as illustrated in Fig.1. In this configuration a capacitor is formed between the upper silicon wafer and the metallized surface of the membrane. Applying a DC voltage between the two conductors of this capacitor produces an electrostatic force field which pulls the membrane inward. The phase shifter so designed is expected to show an extremely low loss equal to the conductor losses of the waveguide walls. Moreover, since the membrane deflection occurs gradually along the waveguide, the phase shifter does not present any significant mismatch.

To demonstrate the feasibility of such phase shifter and characterize its performance, a prototype phase shifter at W-band was designed and under fabrication. In this frequency range we have an HP vector network analyzer which will be use to measure the S-parameters of the prototype phase shifter directly. The test ports of this network analyzer are rectangular waveguides at W-band frequencies. Since the trapezoidal waveguide made by silicon wafers can't be connected to the waveguide flanges of the test set, it was decided to machine the trapezoidal waveguide out of a block of brass with appropriate flanges to mate the test set and fabricate the membrane assembly using silicon micro-machining. This process will be explained in more detail in Section 4. The following tasks were undertaken:

1. Theoretical analysis of general trapezoidal waveguides to determine the dominant mode, mode bandwidth, cutoff frequency and its relationship to the waveguide geometry and dimensions. The results related to this task are provided in Section 3.

2. Characterization of variation of cutoff frequency as a function of the geometrical deformation of the waveguide cross section (membrane displacement). Deter-

mination of the optimum cross section which produces the maximum change in the cutoff frequency for a given membrane displacement.

3. Verification of the theoretical results by constructing a trapezoidal waveguide.

4. Electro-mechanical design and construction of the membrane including calculation of the membrane displacement as a function of applied DC voltage, membrane thickness, width, and modulus of elasticity.

5. Identification of an appropriate membrane and development of a fabrication process. We used different Du Pont Polyimide Coatings to construct relatively large membranes.

6. Construction of a prototype of a membrane-based phase shifter at 94 GHz and characterization of its performance. We have developed the measurement procedures.

3 Theoretical Analysis

3.1 Trapezoidal Waveguide Analysis

As mentioned earlier wet-chemical anisotropic etching creates a trapezoidal groove on a silicon wafer. The small angle of the trapezoid is 54.7° which is determined by the crystallographic nature of silicon crystals. The wide base of the trapezoid (b) and its altitude (h) are to be determined for the desired cutoff frequency. In this section theoretical analysis for characterization of cutoff frequencies, field distribution of dominant mode, and variation of cutoff frequency as a function of base deflection is provided. Analytical solution for the cutoff frequency and field distribution of waveguide structures are available for only a few canonical geometries such as rectangular and circular waveguides. For determination of cutoff frequencies and field distribution of different modes of the trapezoidal waveguide we have to resort to a numerical analysis.

The finite element method offers an efficient numerical procedure for the calculation of the eigenvalues of a waveguide with arbitrary cross section [1]. This technique is well-known and here only a brief discussion of the method is outlined. For homogeneously-filled waveguides the longitudinal component of the electric (TM case) or magnetic (TE case) field, denoted by ψ, satisfies the homogeneous Helmholtz's equation

$$(\nabla^2 + K_c^2)\psi = 0$$

where K_c is the cutoff wavenumber. It is shown that the solution to the Helmholtz's equation minimizes the following functional [2]

$$F(\psi) = \frac{\int\int_S \nabla\psi \cdot \nabla\psi \mathrm{d}s}{\int\int_S \psi^2 \mathrm{d}s} \tag{1}$$

and the minimum is equal to the smallest eigenvalue $\lambda = K_c^2$. To find the minima of the functional the eigenfunction ψ is approximated by a piecewise linear function. In this approximation the cross section of the waveguide is discretized into small triangular elements with unknown values of ψ at each node of the elements. For the eth element the linear function in terms of the node values (ψ_j^e) can be represented by [3]

$$\psi(x,y) = \sum_{j=1}^{3} N_j^e(x,y)\psi_j^e$$

where $N_j^e(x,y)$ are the linear basis function given in terms of the element's nodes $x-y$ coordinates. That is

$$N_j^e(x,y) = \frac{1}{2\Delta^e}(a_j^e + b_j^e x + c_j^e y), \qquad j = 1,2,3$$

$$a_1^e = x_2^e y_3^e - y_2^e x_3^e, \quad b_1^e = y_2^e - y_3^e, \quad c_1^e = x_3^e - x_2^e \tag{2}$$

where Δ^e is the area of the triangle given by

$$\Delta^e = \frac{1}{2}(b_1^e c_2^e - b_2^e c_1^e)$$

and the expressions for $a_2^e, \cdots, c_3^e$ are obtained from (2) by cyclic interchange of the subscripts ($1 \to 2, 2 \to 3, 3 \to 1$).

Substituting the piecewise linear function into the functional (1) and searching for the minima by setting $\frac{\delta}{\delta\psi_j^e} = 0$, the following matrix equation is obtained

$$\tilde{\boldsymbol{A}}\tilde{\Psi} = K_c^2\tilde{\boldsymbol{B}}\tilde{\Psi}$$

where the elements of $\tilde{\boldsymbol{A}}$ and $\tilde{\boldsymbol{B}}$ are given by

$$\tilde{A}_{ij}^e = \frac{1}{4\Delta^e}(b_i^e b_j^e + c_i^e c_j^e)$$
$$\tilde{B}_{ij}^e = \frac{\Delta^e}{12}(1 + \delta_{ij})$$

and δ_{ij} is the Kronecker delta. Since some of the nodes are shared among the adjacent elements, the vector $\tilde{\Psi}$ for the unconnected elements must be related to the vector Ψ for connected elements using a connection matrix $\boldsymbol{C}$ [1]. In this case

$$\tilde{\Psi} = \boldsymbol{C}\Psi$$

and the matrix equation takes the following form

$$\boldsymbol{A}\Psi = K_c^2\boldsymbol{B}\Psi \tag{3}$$

where $\boldsymbol{A} = \boldsymbol{C}^t\tilde{\boldsymbol{A}}\boldsymbol{C}$ and $\boldsymbol{B} = \boldsymbol{C}^t\tilde{\boldsymbol{B}}\boldsymbol{C}$. Equation (3) is recognized as the generalized eigenvalue problem which can be solved numerically by a standard method [4].

Applying this numerical solution to the trapezoidal or the deformed trapezoidal waveguide the cutoff frequencies and associated propagation constants can be obtained. Figures 2-a and 2-b, respectively, show the discretized cross sections of a trapezoidal and a deformed trapezoidal waveguide with $b/h = 2$. Since the expected deflection (δ) is only a few percent of the base width b, the deformed cross section is simply modeled by changing the altitude of the trapezoid to $h + \delta$ everywhere except for the corners (see Fig. 2-b). First we investigated the field distributions of the first and second modes of the trapezoidal waveguide. It was found that the first two modes are TE and that the dominant mode field distribution resembles that of the TE_{10} mode of a rectangular waveguide. Figures 3 and 4, respectively, show the field distributions of the dominant and the second TE modes in a trapezoidal waveguide

with $b/h = 2$. Next we considered the variations of the cutoff frequency of the dominant mode as a function of deflection distance δ. Figure 5 shows the normalized cutoff wavelength (λ_c/b) as a function of normalized deflection distance (δ/b) for three different trapezoidal waveguides with different b/h values 1.5, 2, and 3. It is shown that the cutoff frequency of trapezoidal waveguides increases with decreasing b/h and the rate of change of cutoff wavelength with respect to changes in deflection distance is higher for smaller values of b/h. Noting that $b/h = 1.41$ corresponds to a triangular cross section and the fact that the electric field strength is rather weak at the corners, the cutoff frequency does not change much by decreasing b/h when $b/h < 2$. Another important factor in designing a waveguide is the bandwidth of single mode operation. Figure 6 shows the normalized cutoff wavelengths of the first and second modes as a function of normalized deflection distance. It is shown that a single mode operation bandwidth of about 30% can be achieved for a trapezoidal waveguide with $b/h = 2$.

The most important aspect of this analysis is the calculation of phase shift due to deformation of waveguide cross section. Qualitatively Fig. 5 indicates that the cutoff frequency changes considerably with relatively small deflection values. In order to quantify the phase shift property of this device, let us consider the phase difference between two signals one propagating in an undeformed trapezoidal waveguide and the other one propagating in a deformed waveguide with deflection distance δ. The phase difference over a length of one free-space wavelength (λ_0) can be obtained from

$$\Delta\phi = (\beta^d - \beta^u)\lambda_0$$

where

$$\beta^{d,u} = 2\pi\sqrt{(\frac{1}{\lambda_0})^2 - (\frac{1}{\lambda_c^{d,u}})^2}.$$

and superscripts d and u denote deformed and undeformed waveguides respectively. It is obvious that the phase shift is a function of operating wavelength (λ_0) and more phase shift can be obtained if the operating frequency is near the cutoff frequency of the undeformed waveguide. Noting that for $b = 0.679\lambda_0$ the undeformed waveguide is at cutoff, Fig. 7 shows the phase shift per λ_0 length of the waveguide as a function

Material	Si3N4	SiO2	Cr	Au	Polyimide
Young's Modulus (E)	146 GPa	60 GPa	248 GPa	80 GPa	8.3 GPa
Internal stress σ	900 MPa	300 MPa	850 MPa	260 MPa	9 MPa

Table 1: Mechanical properties of materials to be used in the design of extremely thin diaphragms.

of normalized deflection distance for different values of operating frequencies. It is shown that near cutoff ($b = 0.7\lambda_0$), a phase shift as high as 44° per one free-space wavelength of the waveguide length can be achieved for 5% deflection.

3.2 Mechanical Analysis

In order to design a diaphragm capable of large deflection using minimal amount of force, the mechanical properties of the diaphragm material must be known. These include the Young's modulus of elasticity, Poisson's ratio, and internal stress of various thin films that are used in making the diaphragm. Table 1 summarizes the Young's modulus and internal stress of materials that are to be used in the design of an optimum diaphragm. For most practical applications the Poisson's ratio can be assumed 0.3 for all materials used here. The expected diaphragm design includes two or more layers of different materials and effective Young's modulus and stress for the composite diaphragm are needed for the mechanical analysis. The Young's modulus and stress of a multi-layered structure can be obtained, respectively, from:

$$E_e = \frac{\sum_i E_i t_i}{\sum_i t_i},$$

$$\sigma = \frac{\sum_i \sigma_i t_i}{\sum_i t_i}$$

As mentioned earlier, the diaphragm must be designed such that the required deflection occurs with minimal applied electrostatic force. Thus it is obvious that the diaphragm thickness must be as thin as possible and yet durable. The lower surface of the diaphragm in contact with the waveguide groove must be metallized. The thickness of the metal layer is characterized by the conductivity of the metal film. Because of its high conductivity and resistance to corrosion and oxidization, gold will

be used to metallize the surface of the membrane. Noting that the conductivity of gold is 4.1×10^7 $\mho/m$ and a minimum of two skin depth thickness is required to form a metallic surface, at W-band frequencies a minimum of 5000 $\mathring{A}$ gold is needed. Our goal is to design a diaphragm with a thickness thiner than a few microns. In this case the required diaphragm deflections ($\approx 10-100$ μm) is much larger than the thickness of the diaphragm. Therefore the membrane theory instead of the plate theory must be used for calculating the deflection. When the diaphragm is very thin, it can be considered to have zero bending stiffness. Simple analytical solutions exist for thin membrane when deflection is relatively small compared to the membrane thickness [7]. It has been shown that the central deflection of a rectangular membrane under a uniform load distribution can be obtained from [7]

$$\delta = \alpha \frac{P w^4}{E \tau^3}(1-\gamma^2) \tag{4}$$

where P is the applied pressure, τ and w are the membrane thickness and width respectively, γ is the Poisson's ratio, and α is a constant function of length to width ratio of the membrane. For a square membrane $\alpha = 0.0151$ which almost doubles (0.0312) as the ratio of length to width exceed 2. In our application the deflection is expected to be much larger than the membrane thickness (τ) and it should be noted that (4) overestimates the deflection. On the other hand the applied electrostatic force is not uniform and (4) provides an underestimation of deflection in this regard. Although approximate, this formulation gives the order of magnitude of the required voltage. Because of the large deflection and stretching of the diaphragm, the internal stress does not play an important role in the deflection and therefore is neglected. The required pressure generated by a parallel plate capacitor is given by

$$P = \epsilon \frac{V^2}{2(d-\delta)^2} \tag{5}$$

where d is the capacitor gap before membrane deflection and ϵ is the dielectric constant of the medium (in this case $\epsilon = \epsilon_0$). Substituting (5) into deflection formula (4)

$$V^2 = \frac{16\delta(d-\delta)^2 E\tau^3}{\epsilon_0(1-\gamma^2)w^4}$$

This formula relates the applied voltage to the central deflection.

4 Design Parameters and Experimental Results

To demonstrate the feasibility of this technology, design of a W-band phase shifter is considered. For this purpose, a trapezoidal groove was machined out of a brass block. The groove dimensions are chosen to be $b = 2.40\ mm$ and $h = 1.20\ mm$ (see Fig. 8) which corresponds to a cutoff frequency $f_c = 85$ GHz according to Fig. 5 for $b/h = 2$. At each end of the brass block, the trapezoidal cross section was tapered to rectangular grooves with dimensions $2.54\ mm \times 1.25mm$ to mate the standard WR-10 waveguide. After machining the brass block, the groove was gold-plated for higher conductivity. To check the validity of our numerical results, the cutoff frequency of undeformed trapezoidal waveguide was measured by placing a similar block of gold-plated brass (without the groove) over the trapezoidal groove and its S-parameters were measured using an HP vector network analyzer. Figure 9 shows the measured frequency response of the waveguide over the frequency range 75-110 GHz. It is shown that the cutoff frequency is near 85 GHz as predicted. The relatively high return loss near cutoff is caused by the tapered section. Basically the guide wavelength near cutoff is much longer than the length of the tapered section (about 4 mm). Note that this loss is an artifact of rectangular to trapezoidal transition and not the waveguide itself. In fact the insertion of the 4-cm waveguide itself is about 1 dB at 110 GHz. This insertion loss can be further improved by improving the metallic contact between the two pieces making the waveguide. Figure 11 shows the phase of the S_{12} as a function of frequency where the expected phase variation in a waveguide is observable.

With the confidence in our calculation of the design parameters for trapezoidal waveguides, we proceeded with the design of the membrane. This is the process that has taken a lot of time and effort due to the empirical nature of the work. We chose a length of $a = 30\ mm$ and a width of $b = 4\ mm$ for the diaphragm to cover the trapezoidal groove. In reality the length of the membrane is 40 mm to cover the entire waveguide section, however, the flexible portion is limited to 30 mm.

A wider width for the membrane is chosen to lower the required voltage for the desired deflection. So far we have tried the construction of a $1\mu m$-thick combination of silicon-dioxide (SiO_2) and silicon-nitride (Si_3N_4) covered with a layer of 300 $\mathring{A}$ chromium and a layer of 5000 $\mathring{A}$ gold. The silicon-nitride layer has a high tensile stress which is good for planar membranes to avoid rupture [6]. It was soon found out that this membrane would break much sooner before the required maximum deflection $100\mu m$ is reached. Therefore we decided to chose a different membrane with much lower modulus of elasticity and higher yield strength. It was found that very thin membranes of Dupont polyimide which are very flexible may be fabricated for this application. The proposed diaphragm structure is composed of $2\mu m$ polyimide, 300 $\mathring{A}$Cr, and 5000 $\mathring{A}$Au. Therefore the effective Young's modulus of the membrane is 25.3 GPa. Assuming a gap of the order of $d = 200\mu m$ a moderate voltage of about 54 V is required to get $100\mu m$ deflection. It should be mentioned here that the diaphragm will be pulled down at a deflection of about $\delta = 3/5d$.

The process sequence for the diaphragm fabrication is shown in the Figure 11. It starts with a bare silicon wafer on which about 2500 $\mathring{A}$ of thermal oxide is grown. Our experimental results showed that adhesion of polyimide to SiO_2 is not that good and it fails under tensile stress. For this reason 1000 $\mathring{A}$ of aluminum is evaporated on SiO_2 to enhance the adhesion of polyimide to the substrate. Subsequently 2 to $3\mu m$ of polyimide is span on the wafer (Polyimide PI2611 Dupont). The thickness of the polyimide is determine by the angular speed of the spinner. The polyimide surface is then roughened by oxygen plasma and a layer of Cr(300 $\mathring{A}$)/Au(5000 $\mathring{A}$) is evaporated on top. The oxide on the back side of the wafer is then patterned to define the membrane rim. After many trial we have found that the above process is not complete yet. Basically the silicon etchant attacks the polyimide through the metallized surface. The evaporated gold and chromium is not solid and the etchant reaches the polyimide through the microscopic pores. We are in the process of finding a method to protect the front surface. After protecting the front surface the silicon will be etched in tetra methyl ammonium hydroxide TMAH (12.5 % concentration)

at 75 C° until the membrane is released. A buffered HF dip at the end removes the thin oxide and aluminum from the back side of the diaphragm.

References

[1] Silvester, P., "A general high-order finite-element waveguide analysis program," *IEEE Trans. Microwave Theory Tech.*, vol. MTT-17, no. 4, April 1969.

[2] Dettman, J.W., Mathematical Methods in Physics and Engineering, pp. 149-169, New York: Dover, 1988.

[3] Jin, J., The Finite Element Method in Electromagnetics, New York: John Wiley & Sons, 1993.

[4] Wilkinson, J.H., The Algebraic Eigenvalue Problem, New York: Oxford University Press, 1965.

[5] Chu, L.J., "Electromagnetic waves in elliptic hollow pipes of metal," *J. Appl. Phys.*, vol. 9, pp. 583-591, Sept. 1938.

[6] Wolf, S., and R.N. Tauber, Silicon Processing for the VLSI Era,vol. 1, Lattice Press, 1987.

[7] Giovanni, M.D., Flat and Corrugated Diaphragm Design Handbook, pp.211-216, New York: MARCEL DEKKER.

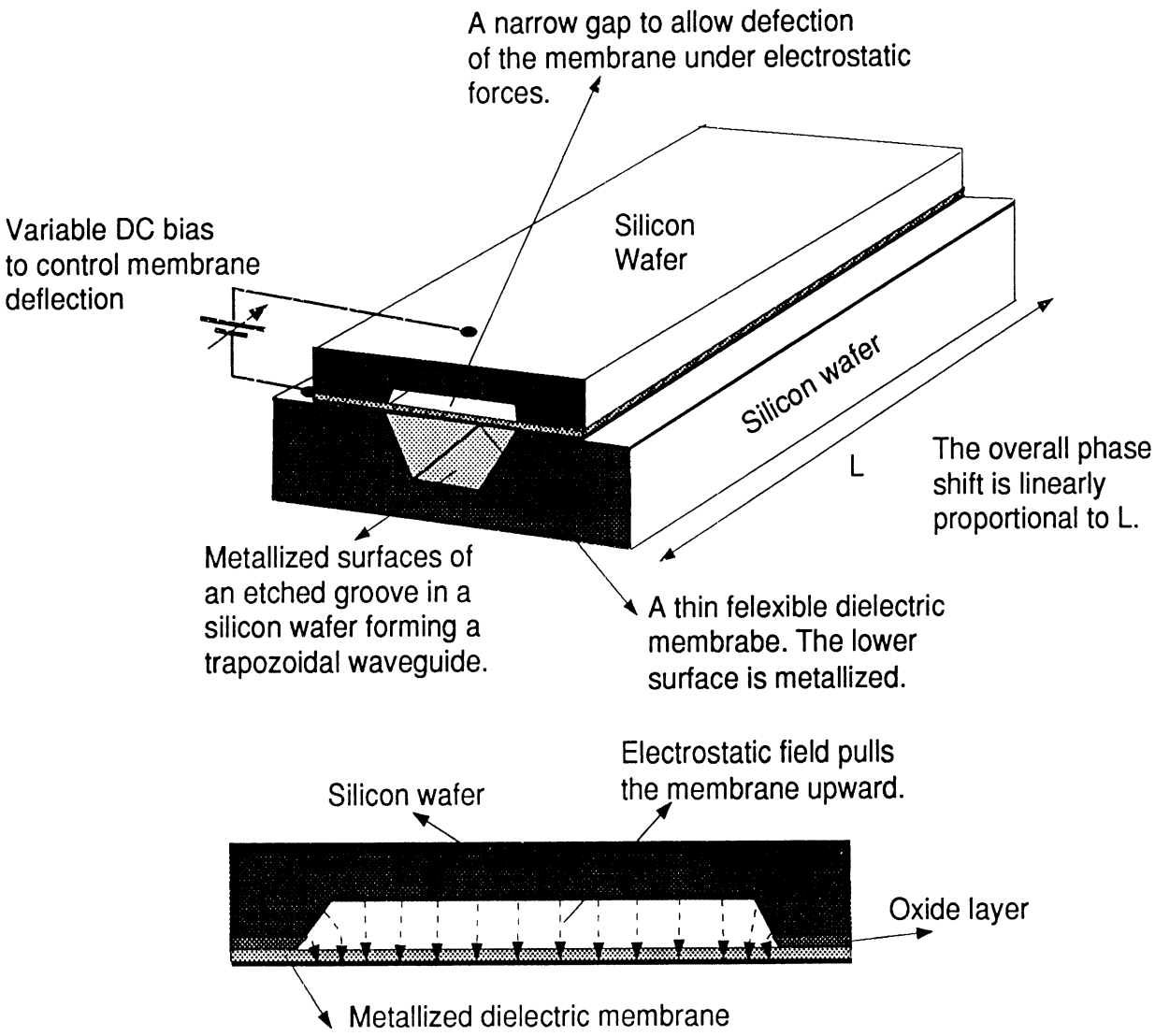

Figure 1: Geometry of the proposed micromachined phase shifter based on a displacement of a waveguide wall.

(a)

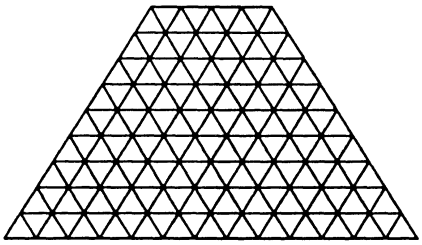

(b)

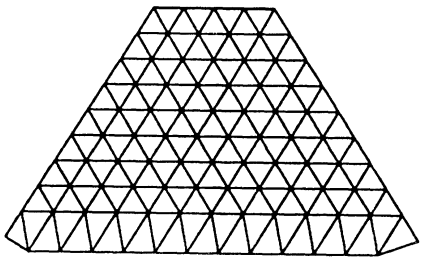

Figure 2: Discretized cross section of an undeformed and deformed trapezoidal waveguide with $b/h = 2$.

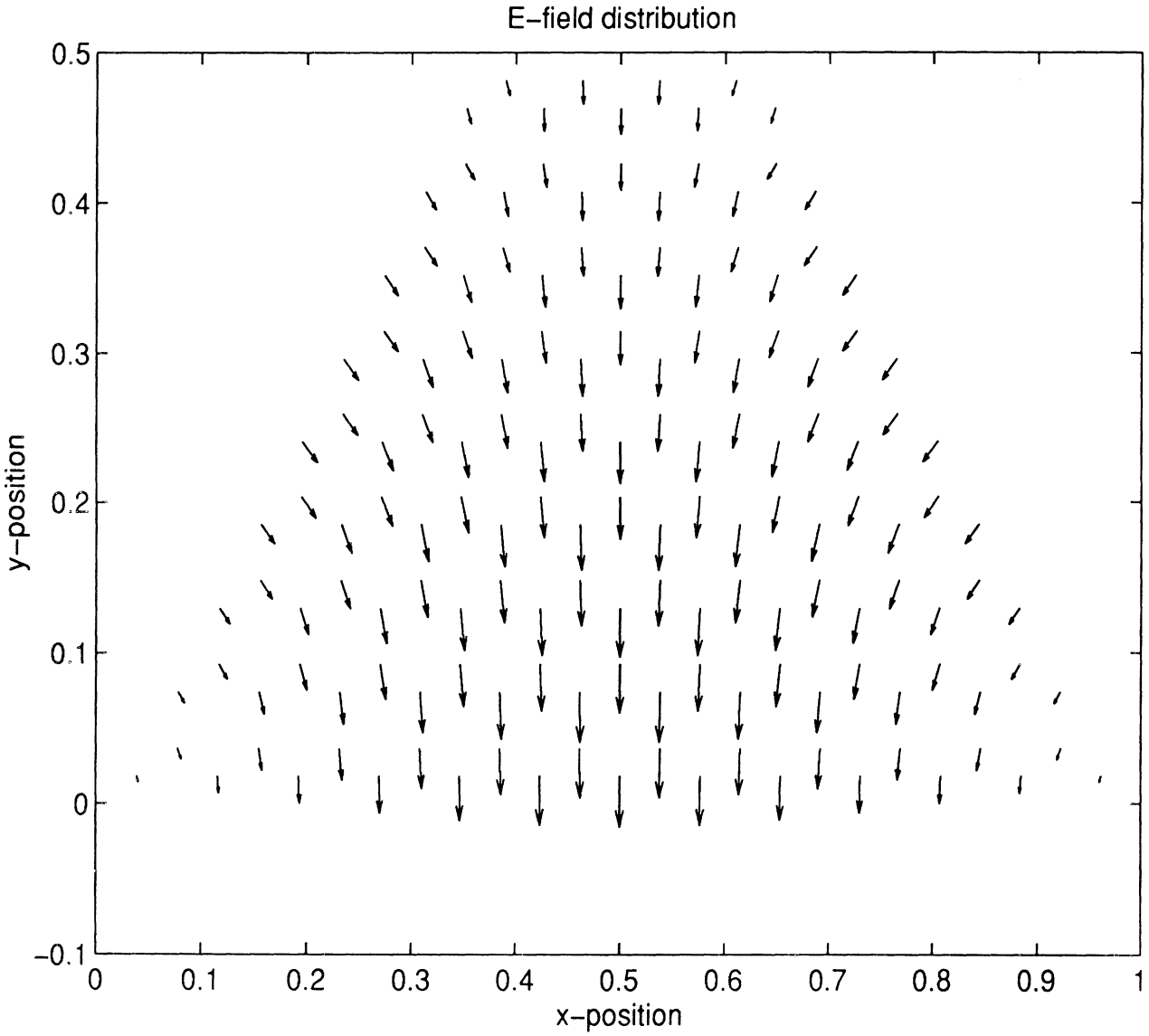

Figure 3: The field distribution of the dominant mode (TE) in a trapezoidal waveguide with $b/h = 2$.

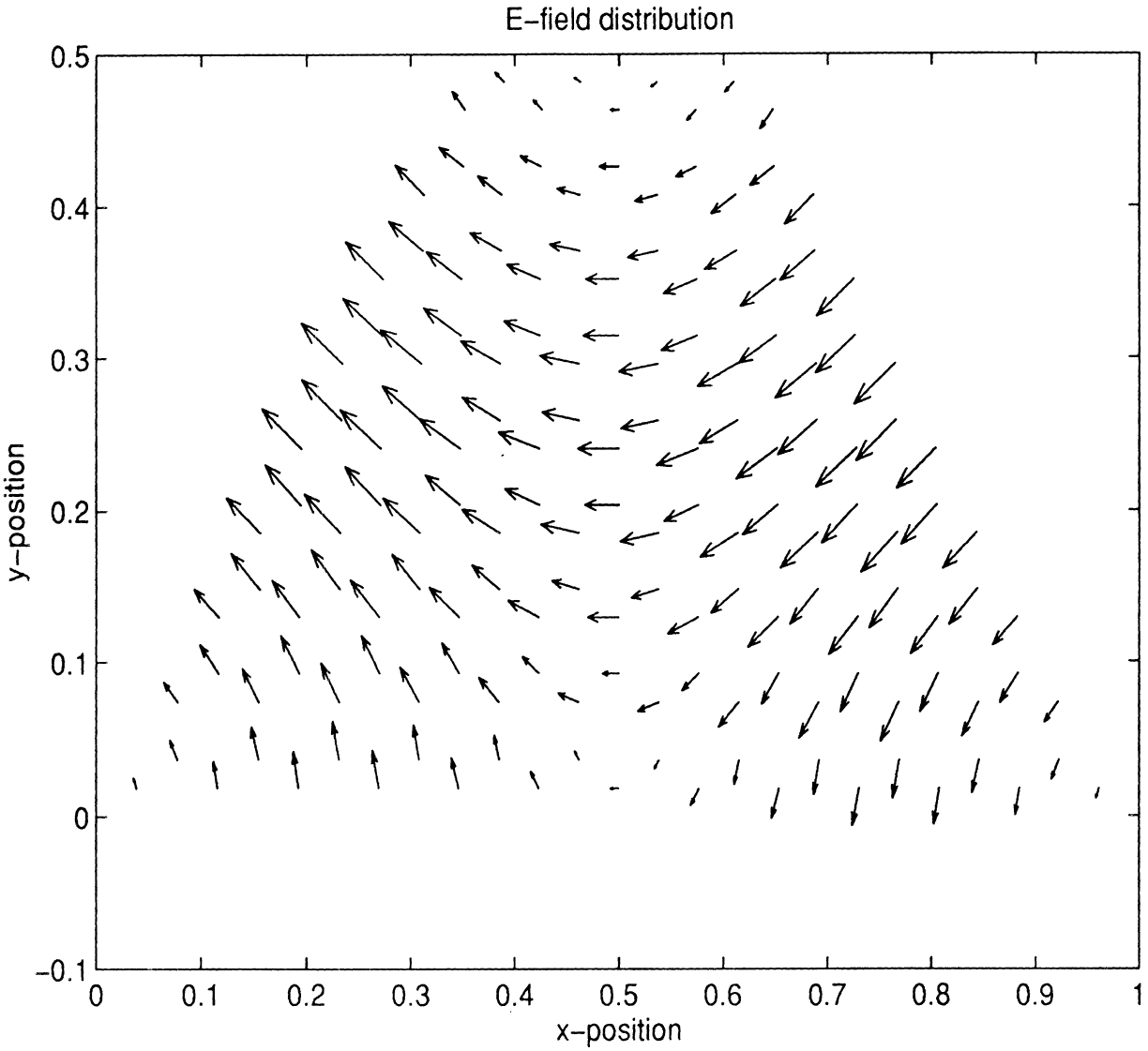

Figure 4: The field distribution of the second mode (TE) in a trapezoidal waveguide with $b/h = 2$.

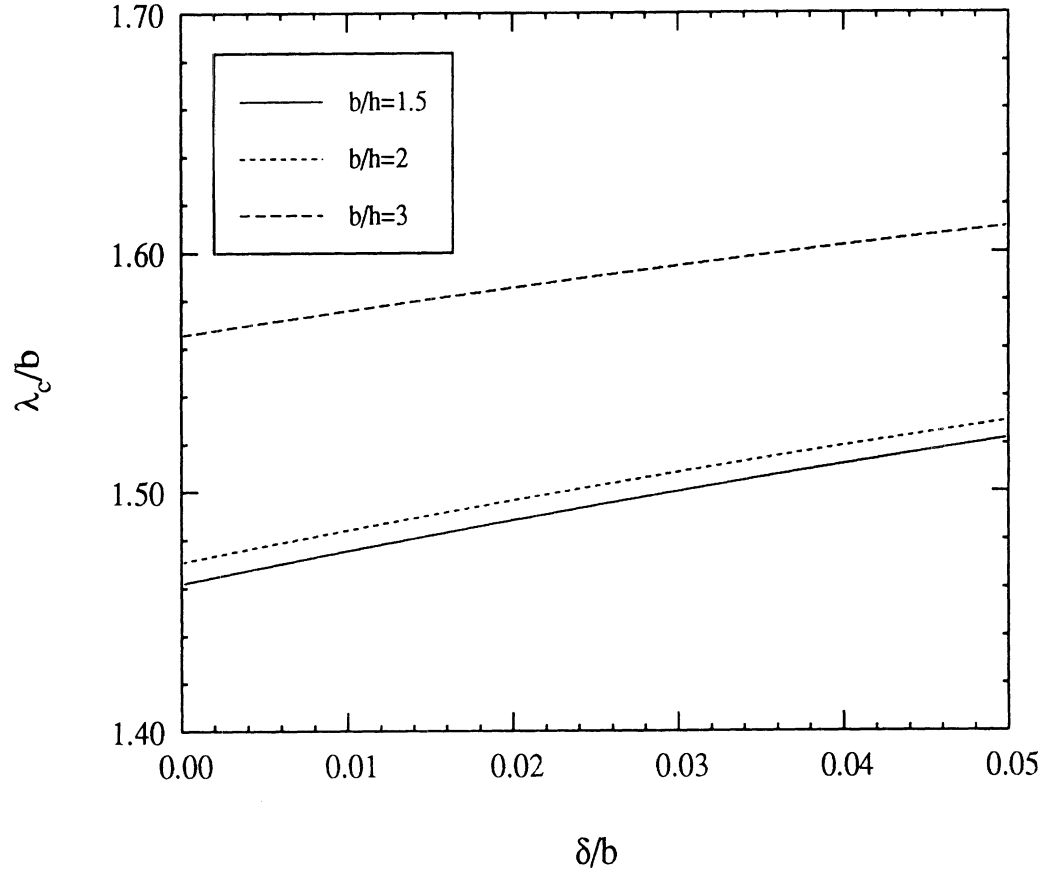

Figure 5: The normalized cutoff wavelength (λ_c/b) as a function of normalized deflection distance (δ/b) for three different trapezoidal waveguides with different b/h values 1.5, 2, and 3.

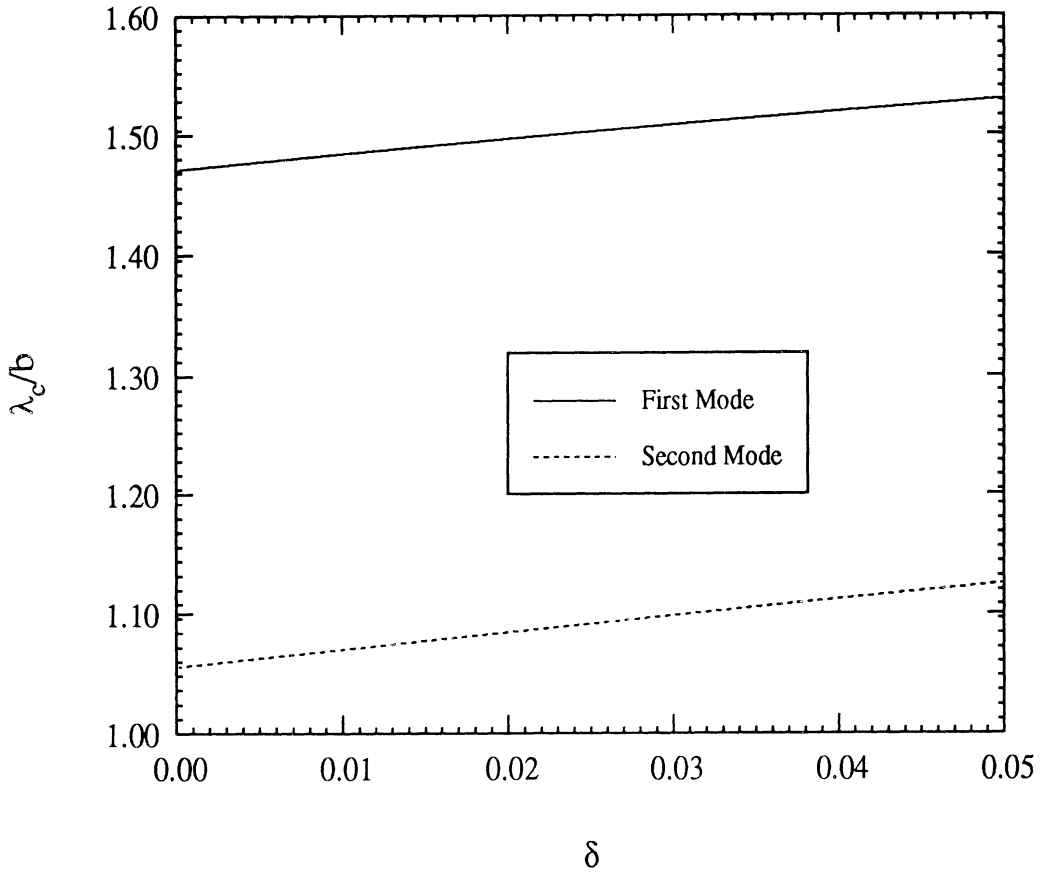

Figure 6: The normalized cutoff wavelength (λ_c/b) as a function of normalized deflection distance (δ/b) for the first two modes of a trapezoidal waveguides with $b/h = 2$

.

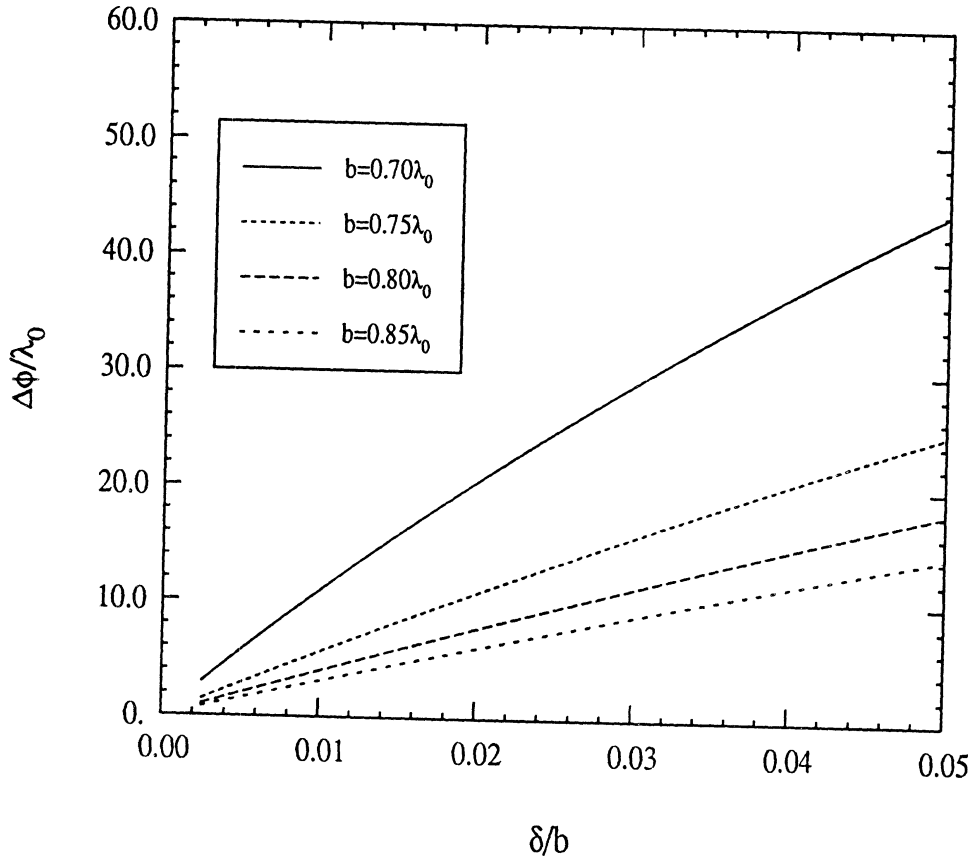

Figure 7: Phase shift per unit free-space wavelength length of a trapezoidal waveguide with $b/h = 2$ at different operating frequencies .

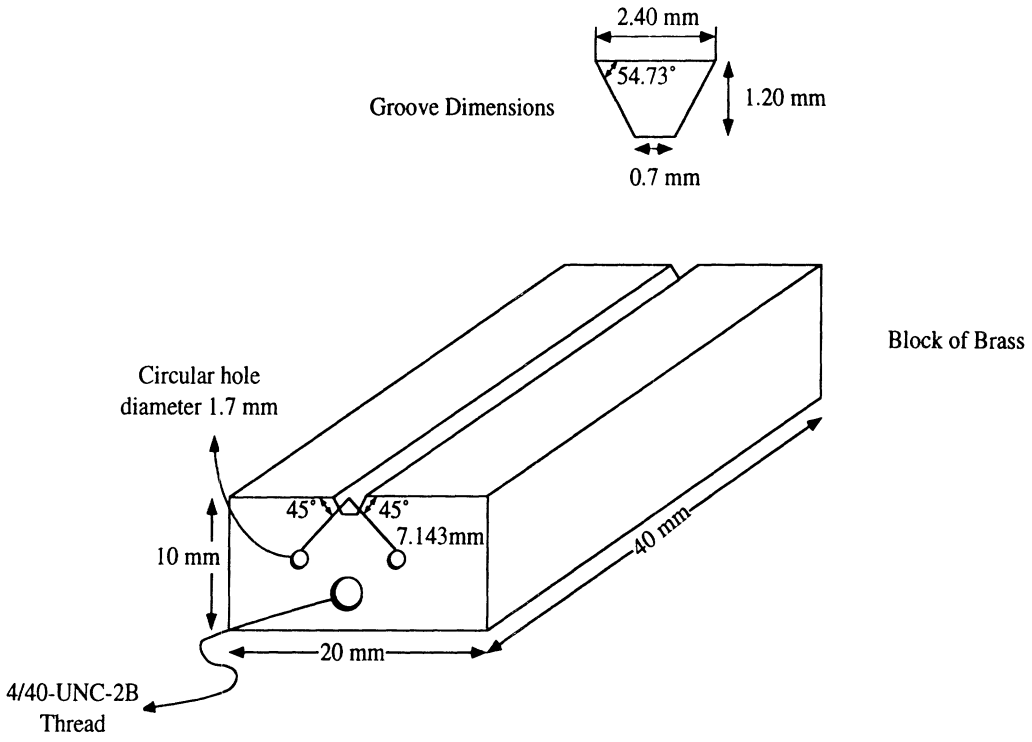

Figure 8: Geometry and dimensions of a trapezoidal waveguide machined out of a brass block designed for operation at W-band frequencies.

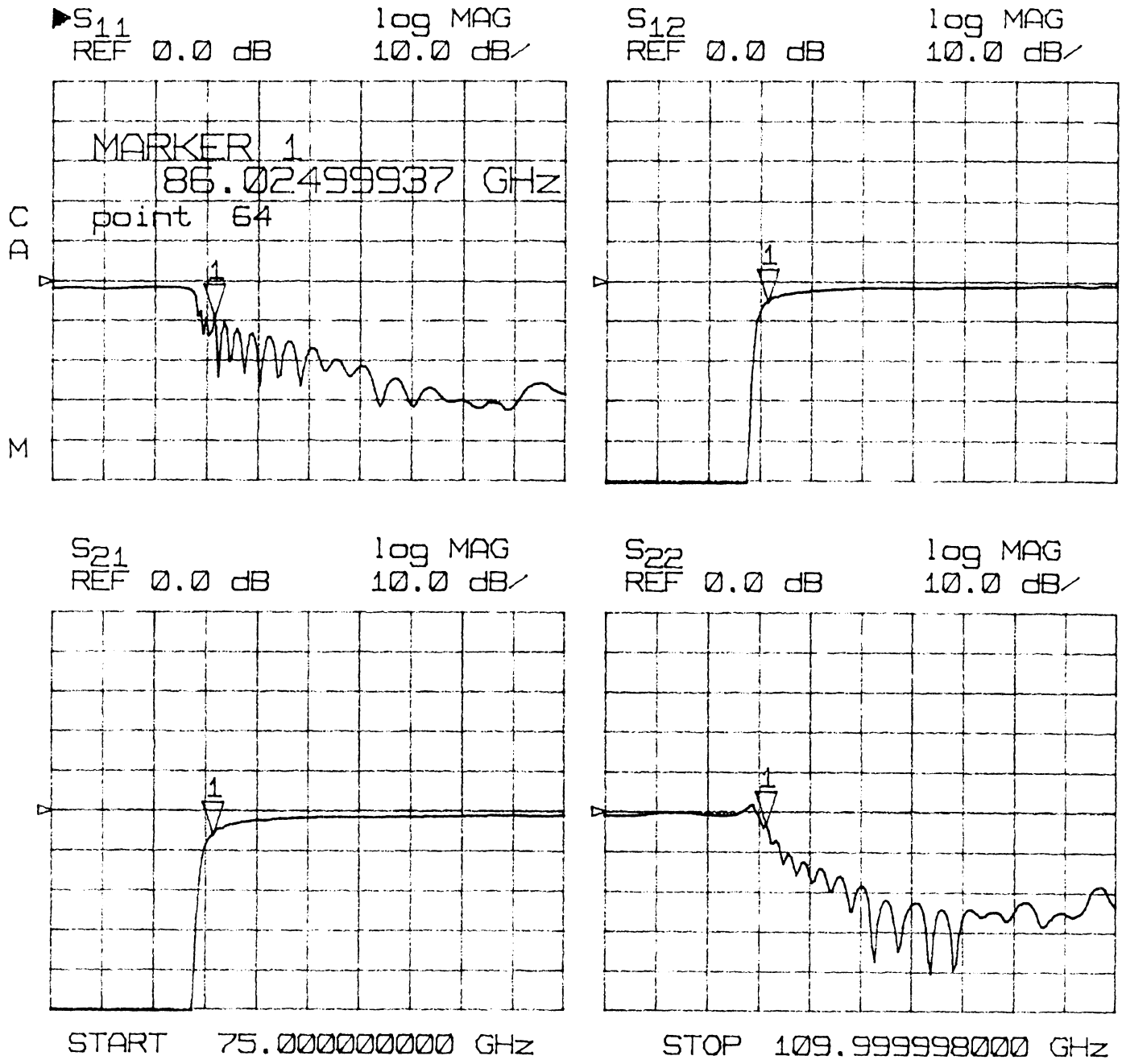

Figure 9: Measured S-parameters of the trapezoidal waveguide over a frequency range 75-110 GHZ.

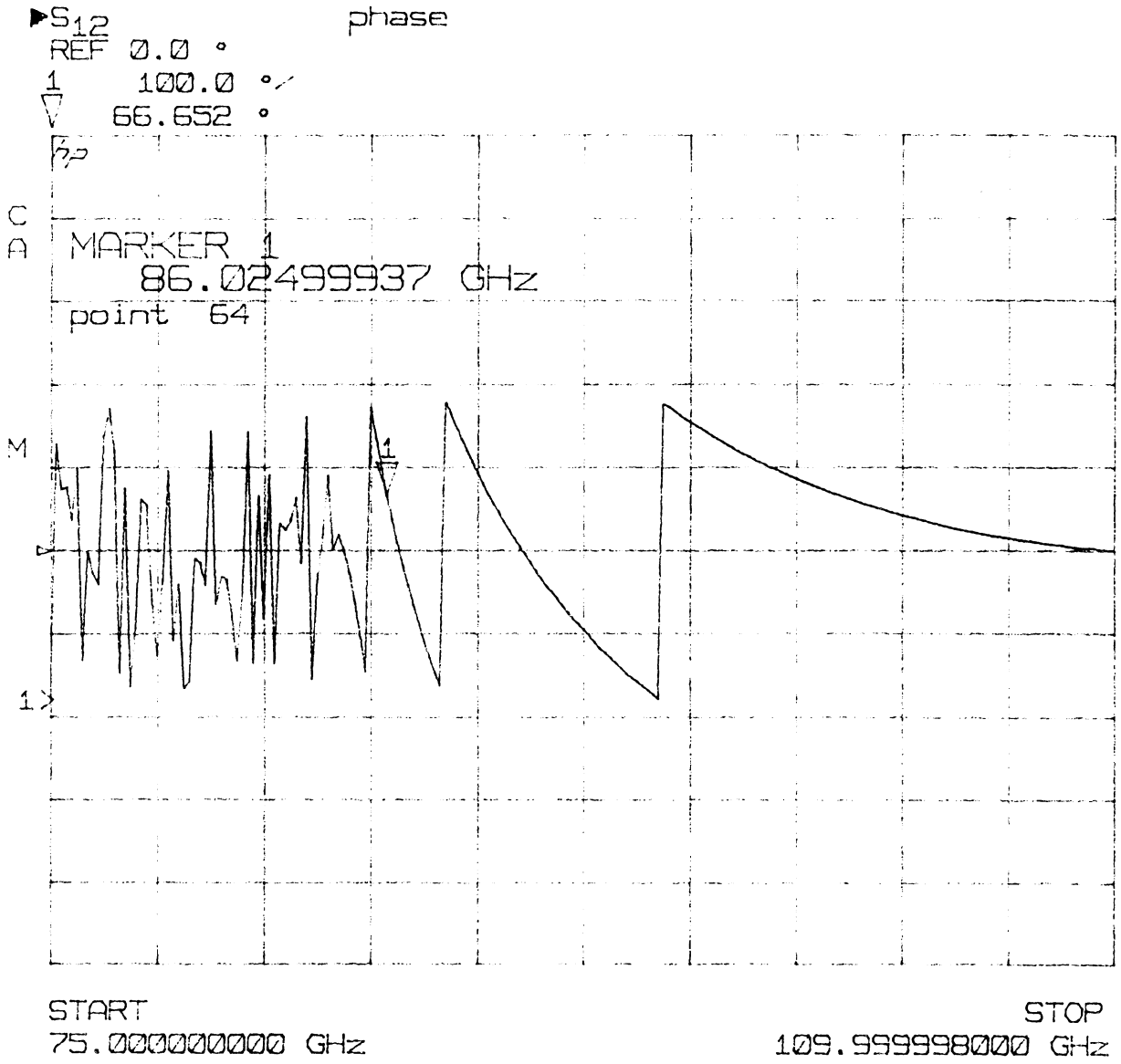

Figure 10: Measured phase response of S_{21} of the trapezoidal waveguide over a frequency range 75-110 GHZ.

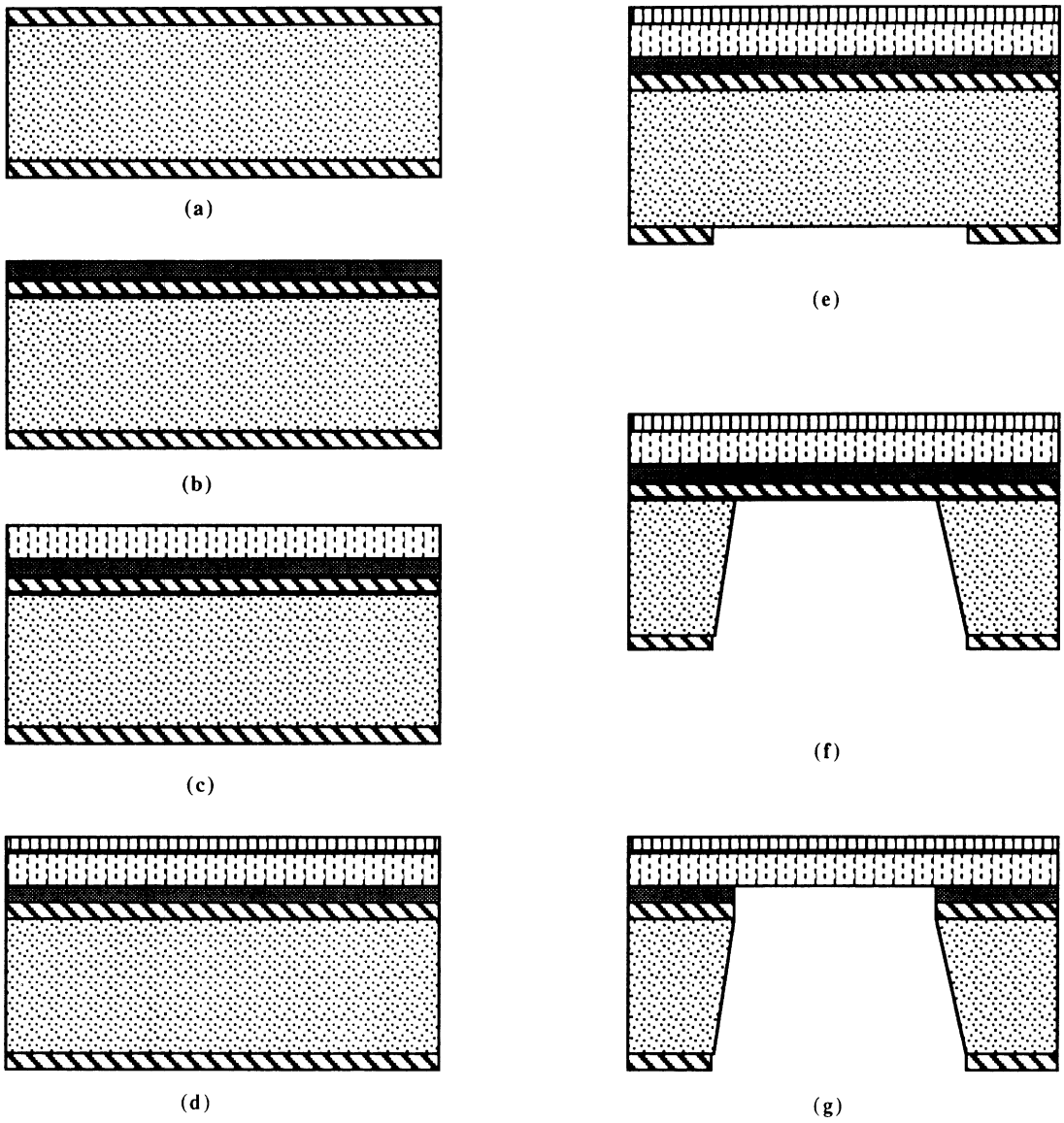

Figure 11: The proposed process sequence for fabrication of a polyimide membrane.